Mechanics in Nano-Engineering 1(1) (2027) 36-57

Ministry of Science, Research and Technology
University of Bonab

Mechanics in Nano-Engineering

journal homepage: https://mneng.ubonab.ac.ir/

Mechanics in NANO-ENGINEERING

Numerical Simulation of Mixed Convection Heat Transfer of ZnO–Water Nanofluid in a Rectangular Cavity with Moving Walls

Pirouz Ghaderi[a,b]

[a] Department of Mechanical Engineering, Urmia University of Technology, Urmia, Iran
[b] Urmia Region Petroleum Products Distribution Company

ARTICLE INFO

Article history:
Received 9 15 2026
Received in revised form 10 16 2026
Accepted 11 6 2026

Keywords:
Mixed convection;
ZnO–water nanofluid;
Rectangular cavity;
Oppositely moving walls;
Nusselt number;
Friction coefficient

ABSTRACT

This study numerically investigates steady, two-dimensional, laminar mixed convection of a ZnO–water nanofluid in a rectangular cavity with an aspect ratio of 2. The upper and lower horizontal walls move in opposite directions with equal dimensionless velocities, while being maintained at different temperatures; the vertical sidewalls are stationary and adiabatic. The governing equations are solved using a characteristic-based numerical method combined with artificial compressibility, and the nanofluid is modeled as a single-phase mixture with effective thermophysical properties. Simulations are conducted at Re = 16, Gr = 4, and Pr = 6.161 for nanoparticle volume fractions of 0%, 2%, 4%, and 6%, with viscous dissipation neglected. The main contribution of this work is the comparative assessment of local and average heat transfer and wall friction on both moving walls, providing insight into the different responses of the hot and cold boundaries to nanoparticle addition. The results reveal that increasing the nanoparticle concentration enhances heat transfer along the upper wall, increasing its average Nusselt number from 11.16 for pure water to 11.87 at 6% concentration. In contrast, the average Nusselt number on the lower wall decreases from 8.48 to 7.16 at 2% concentration, followed by a slight recovery to 7.40 at 6%. Meanwhile, the average friction coefficient increases from 1.00 to 1.65 on both walls. These findings demonstrate that nanoparticle addition produces distinct thermal responses at the two moving boundaries while consistently increasing the hydrodynamic resistance. The results highlight the importance of evaluating heat transfer and wall friction simultaneously when selecting nanoparticle concentrations for mixed convection systems.

1. Introduction

Enhancing convective heat transfer while maintaining acceptable hydraulic performance remains an important objective in the design of thermal management systems, heat exchangers, electronic cooling devices, and energy conversion equipment. Conventional heat transfer fluids, including water, generally exhibit relatively low thermal conductivity, which can limit their thermal performance under certain operating conditions. Nanofluids, produced by dispersing nanoscale solid

particles in conventional base fluids, have therefore attracted considerable attention as potential working fluids for improving heat transfer. Previous investigations have demonstrated that nanoparticle addition can modify the effective thermal conductivity, viscosity, density, and specific heat capacity of the resulting suspension, thereby influencing both the thermal and hydrodynamic characteristics of the flow [1–4]. Nevertheless, the extent of heat transfer enhancement depends on the nanoparticle material, particle concentration, flow regime, and thermal boundary conditions; consequently, an increase in thermal conductivity does not necessarily translate into an equivalent improvement in convective heat transfer.

Mixed convection arises from the simultaneous action of externally imposed fluid motion and buoyancy forces associated with temperature-induced density variations. This mechanism is particularly relevant to cavity flows, where the movement of one or more walls can interact with natural convection to produce complex flow structures and nonuniform temperature distributions. The relative importance of forced and natural convection is commonly characterized by the Richardson number, which compares buoyancy effects with inertial effects. A comprehensive review by Izadi et al. [5] classified research on mixed convection of nanofluids in different enclosure geometries and highlighted the importance of nanoparticle concentration, cavity configuration, and flow conditions in determining thermal performance. The review also emphasized that the potential benefits of nanofluids must be considered alongside their associated hydraulic penalties.

Lid-driven cavities have been widely used as benchmark configurations for investigating shear-driven flow and mixed convection because their boundary conditions can be controlled systematically. In such configurations, moving walls generate forced convection, whereas imposed temperature differences establish buoyancy-driven circulation. Muthtamil Selvan [6] investigated mixed convection in a lid-driven cavity filled with nanofluid, considering moving horizontal walls maintained at different temperatures and insulated vertical walls. Related investigations have extended this configuration to two-sided lid-driven cavities, where the direction and relative velocity of the moving boundaries influence the internal circulation and heat transfer characteristics. Jmai et al. [7] examined the effects of different wall-speed ratios on mixed convection in a partially heated, two-sided lid-driven cavity filled with Cu–water nanofluid. Their findings demonstrated that wall motion and the relative strength of buoyancy can be used to control the flow field and heat transfer rate.

Further research has considered more complex cavity geometries and thermal boundary conditions. Boulahia et al. [8] numerically studied mixed convection of different nanofluids in a two-sided lid-driven square cavity containing triangular heating elements, examining the effects of Richardson number, nanoparticle concentration, particle size, and particle type. Their results showed that the

heat transfer response depends on both the fluid properties and the arrangement of the moving walls and heat sources. Similarly, numerical simulations of double lid-driven cavities using the lattice Boltzmann method have investigated the combined effects of nanoparticle volume fraction and nonuniform thermal boundary conditions [9]. These studies illustrate that the thermal behavior of a nanofluid-filled enclosure cannot be evaluated solely from its effective thermal conductivity; the resulting flow structure and the interaction between the moving boundaries and thermal gradients must also be considered.

The influence of cavity geometry, wall motion, and nanoparticle properties has also been investigated in more recent studies. Nazari and Akbari [10] examined mixed convection of a non-Newtonian nanofluid in a cavity with two oppositely moving walls while accounting for variable thermophysical properties. Their results indicated that the effect of nanoparticle concentration on the average Nusselt number may be nonmonotonic under particular flow conditions. Keklikcioğlu Çakmak et al. [11] numerically investigated mixed convection of Al_2O_3–water nanofluid in a lid-driven cavity using a finite-volume method and a higher-order treatment of convective terms. Their work further demonstrated the relevance of numerical discretization and flow conditions when predicting nanofluid heat transfer. These findings suggest that the influence of nanoparticles should be assessed for the specific configuration under consideration rather than generalized across different cavity geometries and operating regimes.

The scope of research on nanofluid-filled cavities has subsequently expanded to include unsteady wall motion, nonuniform heating, complex geometries, and multiphysics effects. Valizadeh Ardalan et al. [12] investigated unsteady mixed convection of Cu–water nanofluid in an oscillatory lid-driven enclosure using the lattice Boltzmann method. Aljabair et al. [13] studied mixed convection in a sinusoidal lid-driven cavity with nonuniform wall-temperature distribution and demonstrated the importance of wall geometry and thermal boundary conditions in determining the heat transfer characteristics. Alsabery et al. [14] investigated the effects of a two-phase hybrid-nanofluid model in a wavy lid-driven cavity containing a localized solid block. Their study highlighted the influence of nanoparticle transport modeling and internal geometric features on the predicted flow and thermal fields. More recently, Nawafleh et al. [15] examined combined convection in a lid-driven cavity containing CuO–water and Al_2O_3–water nanofluids under different wall-temperature distributions. Collectively, these investigations demonstrate the continuing interest in understanding how nanoparticle characteristics and boundary conditions interact to determine the thermal performance of confined flows.

Recent studies have continued to explore mixed convection and heat transfer in nanofluid-filled cavities with moving boundaries. Souayeh [16] numerically investigated magnetohydrodynamic

mixed convection and entropy generation in a double lid-driven cavity containing a ternary hybrid nanofluid. The study examined the effects of the magnetic field, Richardson number, nanoparticle volume fraction, and lid-velocity ratio on the flow and thermal characteristics. Mliki et al. [17] analyzed MHD mixed convection of a nanofluid in a double-lid-driven convergent cavity using the lattice Boltzmann method. Their results demonstrated that nanoparticle concentration and Reynolds number can enhance the average Nusselt number, whereas the magnetic field suppresses heat transfer. More recently, Loukopoulos et al. [18] investigated transient mixed convection of an electrically conducting micropolar nanofluid in a double lid-driven square cavity using a two-phase model. Their work considered the combined effects of nanoparticle transport, microrotation, and magnetic forces on heat and mass transfer. In addition, Cao et al. [19] studied mixed convection of a water–silver nanofluid in a circular lid-driven cavity and demonstrated that the heat transfer characteristics depend on nanoparticle concentration and the position of the moving cold boundary. Although these studies provide valuable insights into nanofluid convection in moving-boundary enclosures, the effects of nanoparticle concentration on the separate heat transfer and friction characteristics of two oppositely moving, differentially heated horizontal walls in a rectangular cavity remain worthy of further investigation.

Despite the extensive research on mixed convection in nanofluid-filled lid-driven cavities, the combined effects of nanoparticle concentration on heat transfer and wall friction at two oppositely moving, differentially heated horizontal walls have not been sufficiently clarified for the rectangular cavity configuration considered in this study. In particular, previous investigations have addressed various cavity geometries, nanofluid compositions, wall-motion arrangements, and thermal boundary conditions; however, a direct comparison of the thermal and hydrodynamic responses of the two moving walls under identical operating conditions remains of interest. The present study addresses this issue by numerically investigating steady, two-dimensional, laminar mixed convection of ZnO–water nanofluid in a rectangular cavity with an aspect ratio of 2. The upper and lower walls move in opposite directions and are maintained at different temperatures, whereas the vertical sidewalls are stationary and thermally insulated. A single-phase nanofluid model is employed, and the governing equations are solved using a characteristic-based numerical method combined with artificial compressibility. Four nanoparticle volume fractions (0%, 2%, 4%, and 6%) are considered at fixed Reynolds and Grashof numbers. The principal contribution of this work is the simultaneous evaluation and comparison of local and average Nusselt numbers and friction coefficients along both moving walls. This approach makes it possible to identify whether nanoparticle addition affects the heat transfer performance of the hot and cold walls in a similar manner and to quantify the associated increase in wall friction. The findings provide a more

comprehensive understanding of the competing thermal and hydrodynamic effects of ZnO nanoparticle addition in this particular mixed convection configuration.

2. Methods and Material

2.1. Problem Statement and Assumptions

The present study considers steady, two-dimensional, laminar, and incompressible mixed convection flow of a ZnO–water nanofluid inside a rectungle cavity. The flow is driven by the combined effects of an externally imposed shear (forced convection) and buoyancy forces arising from a temperature difference between the cavity walls (natural convection). The Reynolds number is fixed at Re = 16 and the Grashof number at Gr = 4, placing the flow in the laminar mixed convection regime with weak but perceptible buoyancy effects. The nanofluid is treated as a single-phase fluid, assuming that the nanoparticles are uniformly dispersed and in thermal equilibrium with the base fluid, with no slip between the phases. Thermophysical properties of the nanofluid are evaluated from the base fluid and nanoparticle properties using appropriate mixture models. The cavity walls are assumed to be impermeable and no-slip, and the boundary conditions for velocity, pressure, and temperature are imposed consistently to guarantee numerical stability and accuracy.

The computational domain is a two-dimensional rectangular cavity with an aspect ratio of 2, where the horizontal length is twice the vertical height. The top and bottom walls are moving boundaries: the top wall translates to the right with a dimensionless velocity of $U=+1$ and is maintained at a dimensionless temperature of $\theta=-1$, while the bottom wall translates to the left with a dimensionless velocity of $U=-1$ and is kept at $\theta=+1$. The two vertical sidewalls are stationary, impermeable, and thermally insulated (adiabatic). These boundary conditions create a combined forced–natural convection flow in which the shear-driven motion of the walls interacts with the buoyancy force arising from the temperature difference between the top and bottom walls. The imposed thermal and kinematic conditions are summarized as follows:

- Top wall ($y=H$): $u=+1$, $v=0$, $\theta=-1$
- Bottom wall ($y=0$): $u=-1$, $v=0$, $\theta=+1$
- Left and right walls ($x=0$, $x=L$): $u=0$, $v=0$, $\partial\theta/\partial x=0$

where u and v are the dimensionless velocity components in the x- and y-directions, respectively, and θ is the dimensionless temperature. No-slip conditions are applied at all solid walls.

2.2. Governing Equations

In numerical simulations of nanofluids, the mixture is often treated as a single-phase fluid, with its thermophysical properties determined from those of the base fluid and the dispersed nanoparticles. The governing equations—continuity, momentum, and energy—are expressed in dimensionless, matrix form as follows [11]:

$$\frac{\partial Q}{\partial t}+\frac{\partial F}{\partial x}+\frac{\partial G}{\partial y}=\frac{\partial R}{\partial x}+\frac{\partial S}{\partial y}+H$$

$$Z=\begin{bmatrix} p \\ u \\ v \\ T \end{bmatrix},\quad F=\begin{bmatrix} \beta u \\ p+u^2 \\ uv \\ (T-Ec\ p)u \end{bmatrix},\quad G=\begin{bmatrix} \beta v \\ uv \\ p+v^2 \\ (T-Ec\ p)v \end{bmatrix},\quad R=\frac{1}{\mathrm{Re}}\begin{bmatrix} 0 \\ \frac{\partial u}{\partial x} \\ \frac{\partial v}{\partial x} \\ \frac{1}{\mathrm{Pr}}\frac{\partial T}{\partial x} \end{bmatrix},$$

$$S=\frac{1}{\mathrm{Re}}\begin{bmatrix} 0 \\ \frac{\partial u}{\partial y} \\ \frac{\partial v}{\partial y} \\ \frac{1}{\mathrm{Pr}}\frac{\partial T}{\partial y} \end{bmatrix},\quad H=\begin{bmatrix} 0 \\ 0 \\ \frac{Gr}{\mathrm{Re}^2}T \\ \frac{Ec}{\mathrm{Re}}\Phi \end{bmatrix},\quad \Phi=\left(\frac{\partial u}{\partial y}+\frac{\partial v}{\partial x}\right)^2+2\left(\left(\frac{\partial u}{\partial x}\right)^2+\left(\frac{\partial v}{\partial y}\right)^2\right), \tag{1}$$

The continuity equation enforces mass conservation, the momentum equations (Navier–Stokes) describe the dynamic behavior of the viscous fluid under pressure and buoyancy forces, and the energy equation governs the temperature distribution and heat transfer. The buoyancy term is incorporated into the momentum equation through the Boussinesq approximation, in which density variations are retained only in the body-force term and are related to the temperature difference via the volumetric expansion coefficient. The dimensionless parameters governing the problem—Reynolds number, Grashof number, and Prandtl number—appear naturally in the non-dimensionalized equations and control the relative importance of inertia, buoyancy, and thermal diffusion.

2.3. Nanofluid Thermophysical Properties

The subsequent equations are applied to calculate the nanofluid characteristics [11]. The density and specific heat capacity of the nanofluid are obtained from the volume-fraction-weighted mixture rule, while the viscosity and thermal conductivity are evaluated using appropriate correlations that account for the nanoparticle concentration. The volumetric expansion coefficient, which governs

the buoyancy force, is expressed as a mixture of the base-fluid and nanoparticle contributions. These property models are summarized below:

$$\frac{\rho_{nf}}{\rho_{bf}}=1-C+C\frac{\rho_p}{\rho_{bf}};\qquad \frac{\mu_{nf}}{\mu_{bf}}=1+CNv;\qquad \frac{\left(\rho C_p\right)_{nf}}{\left(\rho C_p\right)_{bf}}=1-C+C\frac{\left(\rho C_p\right)_p}{\left(\rho C_p\right)_{bf}};$$
$$\frac{k_{nf}}{k_{bf}}=1+CNc;\qquad \frac{\beta_{nf}}{\beta_{bf}}=\frac{\rho_{nf}}{\rho_{bf}}\left[\left(1-C\right)+C\frac{\left(\rho\beta\right)_p}{\left(\rho\beta\right)_{bf}}\right]. \tag{2}$$

The friction factor and the Nusselt number, used to quantify the hydrodynamic and thermal performance of the system, are calculated as [11]:

$$f=\frac{2}{\mathrm{Re}}\frac{\mu_{nf}}{\mu_{bf}}\frac{\partial u}{\partial y}=\frac{2}{\mathrm{Re}}\frac{\mu_{nf}}{\mu_{bf}}\frac{u_2-u_1}{y_2-y_1};\qquad Nu=\frac{2}{\mathrm{Re}}\frac{k_{nf}}{k_{bf}}\frac{\partial T}{\partial y}=\frac{2}{\mathrm{Re}}\frac{k_{nf}}{k_{bf}}\frac{T_2-T_1}{y_2-y_1}. \tag{3}$$

The Nusselt number represents the ratio of convective to conductive heat transfer and serves as the primary indicator of heat transfer intensity. Its local value along the top and bottom walls reveals the spatial distribution of heat transfer, while the average value characterizes the overall thermal performance of the cavity. The friction coefficient, in turn, reflects the wall shear stress distribution and is used to assess the hydrodynamic behavior of the nanofluid flow along the cavity surfaces.

Table 1 presents the thermophysical properties of pure water, solid ZnO nanoparticles, and the resulting ZnO–water nanofluid at nanoparticle volume fractions of φ = 1%, 2%, and 4%, together with the property models and the fixed dimensionless parameters employed in the simulations. The base fluid is pure water, and the dispersed phase consists of ZnO nanoparticles with a mean diameter in the nanoscale range. As the volume fraction increases from 1% to 4%, the nanofluid density rises from 1043.1 to 1181.2 kg/m³, reflecting the substantially higher density of ZnO (5600 kg/m³) compared with water (997.1 kg/m³). In contrast, the specific heat capacity decreases from 4003.3 to 3538.6 J/(kg·K), since the heat capacity of ZnO (495 J/(kg·K)) is considerably lower than that of water (4179 J/(kg·K)). The dynamic viscosity increases only mildly, from 8.99×10^{-4} to 1.056×10^{-3} Pa·s, while the thermal conductivity exhibits a more pronounced enhancement, rising from 0.6455 to 0.7539 W/(m·K) as φ increases; this improvement is attributed to the much higher thermal conductivity of ZnO (29 W/(m·K)) relative to water (0.613 W/(m·K)). The volumetric expansion coefficient decreases slightly with increasing particle loading, from 2.079×10^{-4} to 2.016×10^{-4} K^{-1}, because the expansion coefficient of ZnO (3.0×10^{-6} K^{-1}) is two orders of magnitude smaller than that of water (2.1×10^{-4} K^{-1}). These property variations indicate that, within the dilute range considered here, the addition of ZnO nanoparticles simultaneously enhances the thermal

conductivity and reduces the heat capacity of the mixture, which is expected to influence both the thermal boundary layer development and the buoyancy-driven flow inside the cavity.

Table 1. Thermophysical properties and property models of the ZnO–water nanofluid at φ = 1%, 2%, and 4%.

Property	Water	**ZnO**	**ZnO-water (φ=2%)**	**ZnO-water (φ=4%)**	**ZnO-water (φ=6%)**
Density(kg/m³)	997.1	5600	1089.2	1181.2	1273.3
Specific heat capacity (J/(kg·K))	4179	495	3838.6	3538.6	3206.8
Dynamic viscosity (Pa·s)	8.55×10^{-4}	-	9.47×10^{-4}	1.056×10^{-3}	1.554×10^{-4}
Thermal conductivity (W/(m·K))	0.613	29	0.6797	0.7539	۰,۸۲۸۱
Volumetric expansion coefficient (K^{-1})	2.1×10^{-4}	3.0×10^{-6}	2.058×10^{-4}	2.016×10^{-4}	1.976×10^{-4}

2.4. Numerical Method and Solution Procedure

The governing equations are solved using an in-house Fortran code based on a two-dimensional characteristic-based method. In this approach, the convective terms are discretized along the characteristic lines, which enhances the stability and accuracy of the scheme for incompressible convective heat transfer problems. Since the flow is incompressible, the pressure field is obtained using the artificial compressibility method of Chorin, in which a pseudo-time derivative of pressure is introduced into the continuity equation to couple the pressure and velocity fields. The resulting system is advanced iteratively in pseudo-time until a steady-state converged solution is reached. The discretization is performed on a structured, uniform Cartesian mesh, which is well suited to the square cavity geometry and the laminar flow regime considered here. The iterative solution procedure is monitored through the convergence history of the residuals, and appropriate boundary conditions are applied at all walls to ensure numerical stability and accuracy.

The overall solution algorithm is illustrated in the flowchart of **Fig. 1** and can be summarized in the following steps:

1. **Grid generation:** A structured, uniform Cartesian mesh is generated over the square cavity domain, and the coordinates of the grid nodes are defined.

2. **Initialization:** The velocity components (U, V), pressure (P), and temperature (θ) fields are initialized over the entire domain. Initial values are chosen to be consistent with the imposed boundary conditions.

3. **Boundary conditions:** At each iteration, the velocity, pressure, and temperature boundary conditions are imposed on the cavity walls (no-slip, impermeability, and prescribed thermal conditions).

4. **Convective flux computation:** The convective terms of the momentum and energy equations are discretized along the characteristic lines, and the corresponding fluxes are evaluated at the cell faces.

5. **Viscous and conduction flux computation:** The viscous terms in the momentum equations and the conduction terms in the energy equation are discretized using central differences on the structured mesh.

6. **Pressure–velocity coupling:** The artificial compressibility formulation is used to update the pressure field via the pseudo-time derivative of pressure in the continuity equation, ensuring the divergence-free condition is gradually enforced.

7. **Temporal (pseudo-time) update:** The velocity, pressure, and temperature fields are advanced in pseudo-time using the characteristic-based time integration.

8. **Convergence check:** The residual (error) of the governing equations is computed. If the residual is below a prescribed tolerance (e.g., 10^{-5}), the solution is considered converged and the iteration stops; otherwise, the procedure returns to step 3 and repeats.

9. **Post-processing:** Once convergence is achieved, the velocity, pressure, and temperature fields are exported, and the local and average Nusselt numbers, friction coefficients, and flow/temperature profiles are computed and visualized using Tecplot.

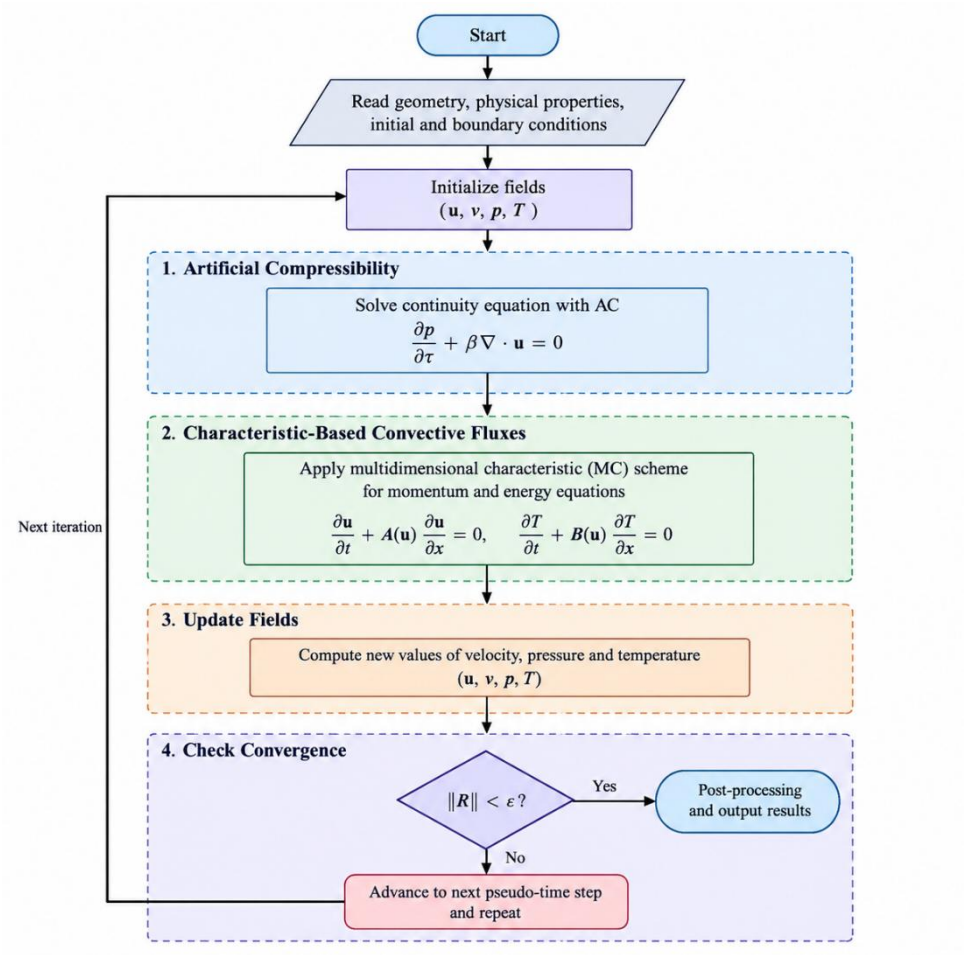


Figure 1. Flowchart of the characteristic-based solution algorithm with artificial compressibility

2.5. Convergence of the Numerical Solution

Convergence plots are crucial in numerical simulations to ensure the reliability and accuracy of the results. They illustrate how the solution evolves over successive iterations during the numerical process. A well-converged solution demonstrates that the residuals—the difference between the calculated values and the governing equations—have decreased sufficiently and stabilized, indicating that the numerical method has reached a steady state. Lack of convergence, or slow convergence, can signify issues with the numerical scheme, boundary conditions, or the problem itself, potentially leading to inaccurate or misleading results. Therefore, presenting convergence plots provides transparency and validates the robustness of the numerical solution.

The convergence history of the numerical solution is presented in Fig. 2, where the error is plotted against the number of iterations on logarithmic scales. The error decreases continuously from approximately 2×10^{-1} to below 10^{-4} as the iterations increase, indicating stable convergence of the numerical solution. At higher iteration numbers, the error reaches the order of 10^{-5}, despite a small fluctuation in the convergence curve. The final error is approximately 10^{-5}, demonstrating that the computational model achieves a sufficiently small residual and reaches a converged solution.

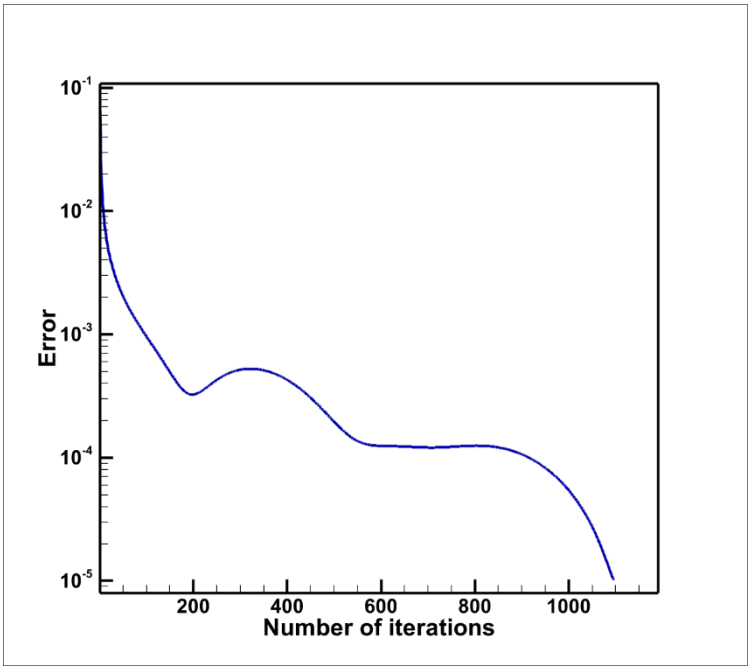


Figure 2. Convergence history of the numerical solution.

2.6. Grid Independence Study

A grid independence study, also known as mesh refinement analysis, is a critical step in validating numerical simulations. It assesses the sensitivity of the solution to the mesh size, ensuring that the results are not significantly affected by the discretization of the computational domain. By systematically increasing the mesh density and observing the changes in the solution, one can determine a mesh size that provides a balance between accuracy and computational cost. Achieving grid independence demonstrates that the solution has converged to a mesh-size-independent state, lending confidence to the reliability and accuracy of the numerical results.

Simulations were performed using mesh sizes ranging from 10,000 to 320,000 elements. The results reveal that the temperature profiles obtained from the 160,000 and 320,000 element meshes exhibit a difference of less than 1% (Fig. 3). This minimal variation indicates that the solution has reached a grid-independent state. Consequently, a mesh size of 160,000 elements was selected as the final mesh for all subsequent simulations, ensuring the accuracy and reliability of the obtained results without excessive computational burden.

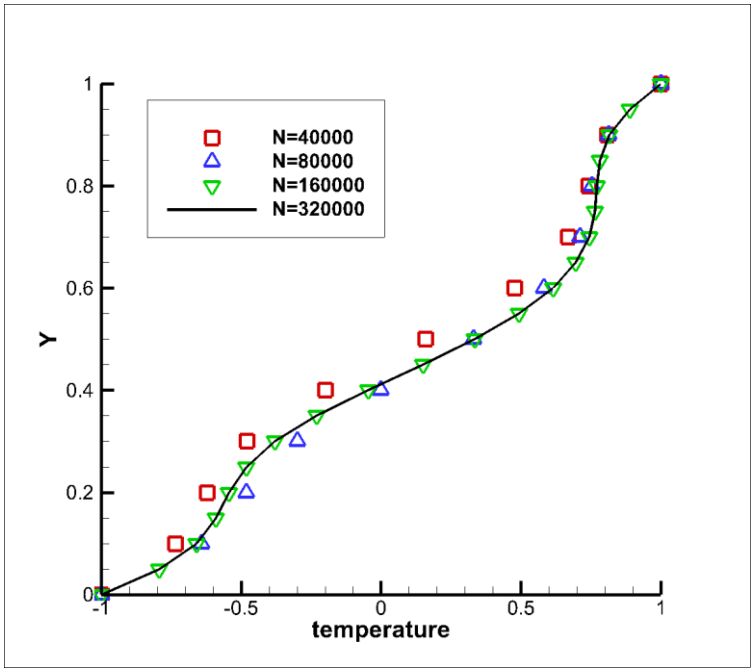


Fig 3- Grid independence (temperature variation along vertical centerline)

2.7. Validation

Validation is a fundamental aspect of scientific research, particularly in numerical modeling. It involves comparing the results of a new model or simulation with existing experimental data or established theoretical solutions. This process ensures that the model accurately represents the physical phenomena being studied and provides reliable predictions. Validation strengthens the credibility of the research and allows for confident interpretation of the results. Without proper validation, the conclusions drawn from a numerical study may be questionable.

To validate the present numerical model and the implemented characteristic-based code, the computed local Nusselt number distribution is compared with the numerical results reported by Adibi et al. [1] under identical mixed convection conditions. As illustrated in Fig. 4, the present results exhibit an excellent agreement with the benchmark data. The Nusselt number profile, including the peak location and the overall trend of variation along the wall, is captured accurately. This strong agreement confirms the reliability and accuracy of the current numerical scheme and the applied boundary conditions for simulating mixed convection of nanofluids in the square cavity.

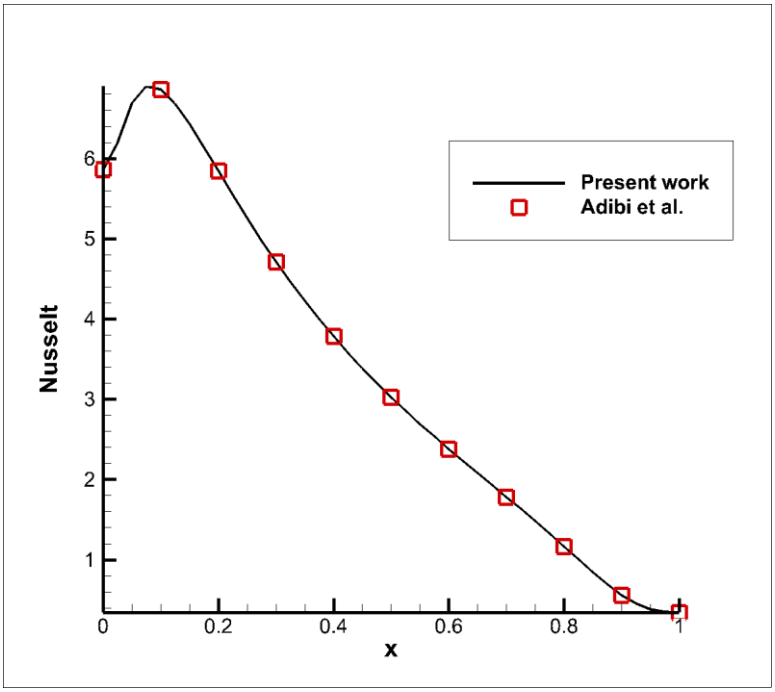


Figure 4. Comparison of the local Nusselt number distribution along the top wall between the present work and the numerical results of Adibi et al. [20].

3. Results and Discussion

This section presents the numerical results for the steady, two-dimensional, laminar mixed convection flow of a ZnO–water nanofluid inside a square cavity. The simulations are performed for a fixed Reynolds number of Re=16, Grashof number of Gr=4, and Prandtl number of Pr=6.161. To isolate the thermal and hydrodynamic effects of the nanoparticles from viscous dissipation, the Eckert number is set to zero (Ec=0). The study examines the influence of nanoparticle volume fraction at four concentrations: ϕ=0 (pure water), 2%, 4%, and 6%.

The results are organized as follows. First, the local Nusselt number distributions along the top and bottom walls are presented to evaluate the heat transfer characteristics at each concentration. Subsequently, the local friction coefficient distributions along the same walls are analyzed to assess the hydrodynamic behavior and wall shear stress. Finally, the average Nusselt numbers and average friction coefficients for both the top and bottom walls are summarized in a table to provide a quantitative comparison of the overall thermal and hydrodynamic performance of the cavity at different nanoparticle loadings.

Figure 5 presents the local Nusselt number distribution along the top wall of the cavity for nanoparticle volume fractions of ϕ=0%, 2%, 4%, and 6%. The top wall moves to the right with a dimensionless velocity of +1 and is maintained at a lower temperature (θ=−1) than the bottom wall (θ=+1). As seen in the figure, the Nusselt number decreases continuously from the left corner (x=0)

toward the right corner (x=2). This behavior is attributed to the combined effects of the wall motion and the thermal boundary layer development: near the left corner, the cold fluid adjacent to the top wall encounters the upward buoyancy-driven flow originating from the heated bottom wall, resulting in a thinner thermal boundary layer and a higher temperature gradient. As the flow progresses to the right, the thermal boundary layer thickens, and the wall shear-driven motion gradually homogenizes the temperature field, leading to a reduction in the local Nusselt number.

Furthermore, the results demonstrate that increasing the nanoparticle volume fraction systematically enhances the local Nusselt number along the entire top wall. At any given axial position, the Nusselt number for ϕ=6% is higher than that for ϕ=4%, which in turn exceeds those for ϕ=2% and ϕ=0%. For example, at the left corner (x=0), the Nusselt number rises from approximately 31.43 for pure water to 33.32 for the 6% nanofluid, corresponding to an enhancement of about 6%. This improvement is primarily due to the higher thermal conductivity of ZnO nanoparticles relative to the base fluid, which enhances heat conduction through the nanofluid and strengthens the convective heat transfer at the wall. Although the addition of nanoparticles also increases the effective viscosity and density of the mixture—which can modify the flow structure and thermal boundary layer—the observed monotonic enhancement confirms that the thermal conductivity effect dominates under the present mixed convection conditions.

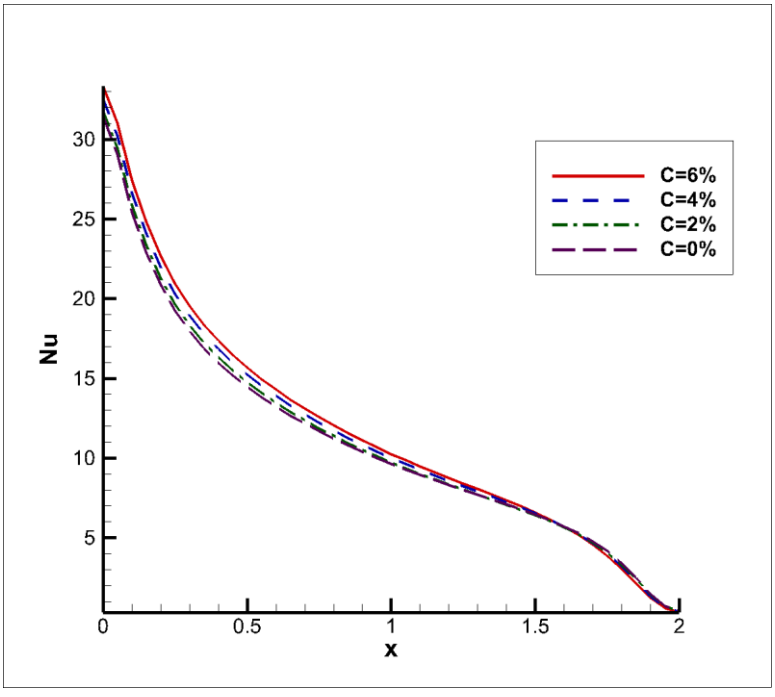


Figure 5. Local Nusselt number distribution along the top wall of the cavity for different ZnO nanoparticle volume fractions (ϕ=0%,2%,4%,6%)

Figure 6 shows the local Nusselt number distribution along the bottom wall of the cavity for nanoparticle volume fractions of ϕ=0%, 2%, 4%, and 6%. The bottom wall moves to the left with

a dimensionless velocity of −1 and is maintained at a higher temperature (θ=+1) than the top wall (θ=−1). In contrast to the top wall, the Nusselt number along the bottom wall increases monotonically from the left corner (x=0) toward the right corner (x=2), where it reaches its maximum value. Near the left corner, the Nusselt number is very small (close to zero), indicating that the thermal boundary layer is thick and the local heat transfer is weak. This is because the leftward motion of the heated bottom wall carries hot fluid away from the left region, while the cold downward flow from the top wall is not yet fully developed there. As the flow progresses to the right, the interaction between the cold descending stream and the heated wall intensifies, thinning the thermal boundary layer and substantially enhancing the local heat transfer. Consequently, the Nusselt number rises sharply near the right corner, reaching values of approximately 26.44, 22.30, 22.90, and 22.92 for ϕ=0%, 2%, 4%, and 6%, respectively.

A notable feature of Fig. 6 is that, unlike the top wall, increasing the nanoparticle concentration generally reduces the local Nusselt number along the bottom wall. For instance, at x=2, the Nusselt number decreases from about 26.44 for pure water to 22.92 for the 6% nanofluid. This reduction can be attributed to the combined effects of increased effective viscosity and reduced specific heat capacity of the nanofluid. The higher viscosity suppresses the buoyancy-driven flow and thickens the thermal boundary layer, while the lower heat capacity reduces the thermal diffusivity of the mixture. These effects outweigh the enhancement in thermal conductivity, leading to a net decrease in the local heat transfer rate at the bottom wall. The non-monotonic variation between ϕ=2% and ϕ=4% (with the 4% case slightly exceeding the 2% case near the right corner) suggests a delicate balance between the competing effects of thermal conductivity enhancement and viscous suppression at intermediate concentrations.

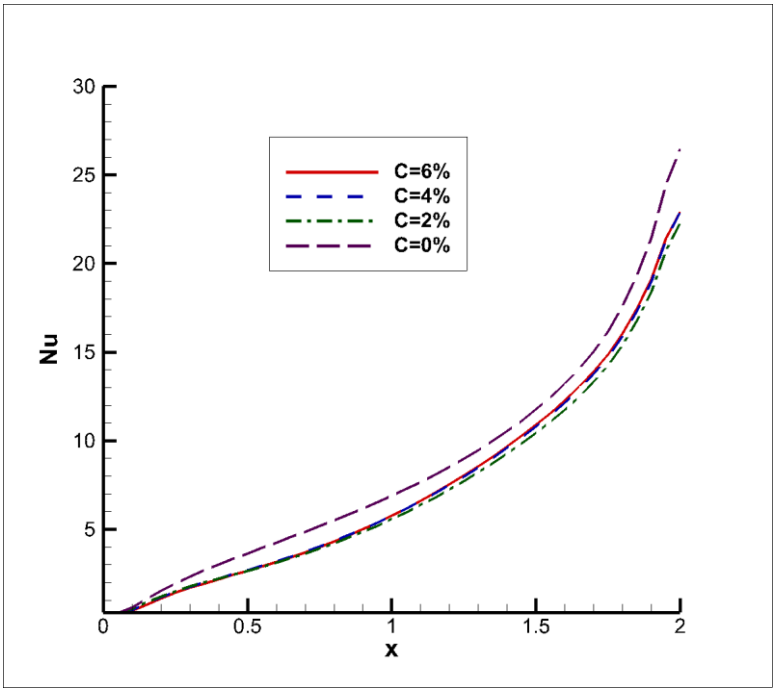


Figure 6. Local Nusselt number distribution along the bottom wall of the cavity for different ZnO nanoparticle volume fractions (ϕ=0%,2%,4%,6%).

Figure 7 illustrates the local friction coefficient distribution along the top wall of the cavity for nanoparticle volume fractions of ϕ=0%, 2%, 4%, and 6%. The friction coefficient exhibits a symmetric U-shaped profile, with maximum values at both corners (x=0 and x=2) and a minimum near the mid-section of the wall (around x≈0.95). At the corners, the no-slip condition combined with the abrupt change in the flow direction and the interaction between the moving wall and the stationary sidewalls produce large velocity gradients, resulting in high wall shear stress and, consequently, elevated friction coefficients. In the central region, the flow is more fully developed and the velocity gradient near the wall is reduced, leading to a minimum in the friction coefficient.

The results further show that increasing the nanoparticle volume fraction systematically increases the local friction coefficient along the entire top wall. For instance, at the right corner (x=2), the friction coefficient rises from 5.00 for pure water to 6.09, 7.18, and 8.26 for ϕ=2%, 4%, and 6%, respectively. This monotonic enhancement is directly attributed to the higher dynamic viscosity of the ZnO–water nanofluid compared to the base fluid. As the particle loading increases, the effective viscosity of the mixture rises, which intensifies the viscous shear stress at the wall and thereby increases the friction coefficient. The position of the minimum friction coefficient shifts only slightly with concentration, indicating that the overall flow structure and the location of the maximum velocity gradient near the wall remain largely unaffected by the nanoparticle loading, while the magnitude of the wall shear stress is significantly amplified.

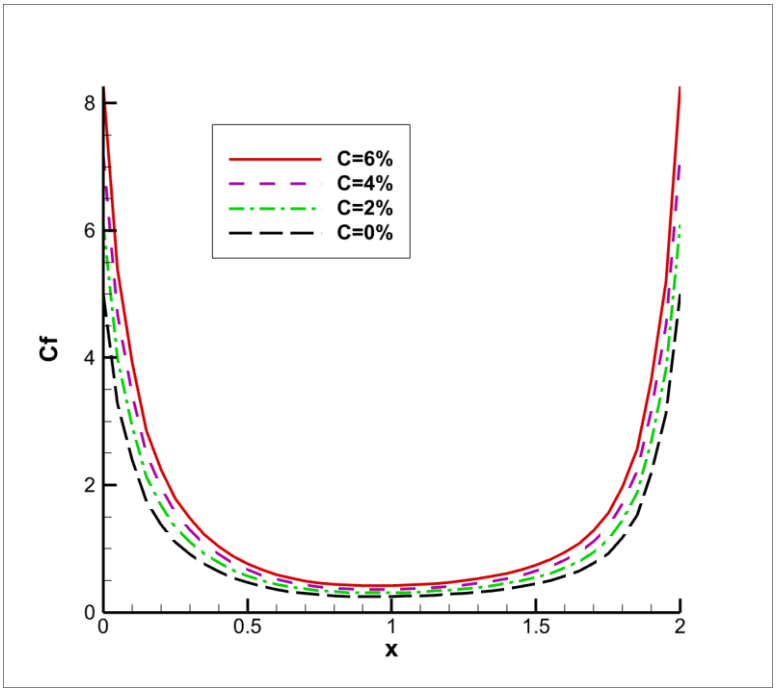


Figure 7. Local friction coefficient distribution along the top wall of the cavity for different ZnO nanoparticle volume fractions (ϕ=0%,2%,4%,6%).

Figure 8 presents the local friction coefficient distribution along the bottom wall of the cavity for nanoparticle volume fractions of ϕ=0%, 2%, 4%, and 6%. Similar to the top wall, the friction coefficient exhibits a U-shaped profile, with maximum values at both corners (x=0 and x=2) and a minimum near the mid-section of the wall (around x≈1.05). The high friction coefficients at the corners are caused by the large velocity gradients resulting from the no-slip condition and the interaction between the moving wall and the stationary sidewalls. In the central region, the velocity gradient near the wall is reduced, leading to a minimum in the friction coefficient. The slight shift of the minimum toward the right side (x≈1.05) compared to the top wall (x≈0.95) reflects the opposite direction of the bottom wall motion (leftward) and its different interaction with the buoyancy-driven flow.

The results clearly demonstrate that increasing the nanoparticle volume fraction monotonically enhances the local friction coefficient along the entire bottom wall. For instance, at the left corner (x=0), the friction coefficient increases from 5.00 for pure water to 6.09, 7.18, and 8.26 for ϕ=2%, 4%, and 6%, respectively. Similarly, at the right corner (x=2), the same values are recovered due to the symmetry of the boundary conditions at the two corners. This enhancement is primarily attributed to the higher effective viscosity of the ZnO–water nanofluid compared to the base fluid. As the nanoparticle concentration increases, the viscous shear stress at the wall intensifies, leading to a higher friction coefficient. The consistent increase in Cf across the entire wall confirms that

the hydrodynamic penalty associated with nanoparticle addition is significant under the present mixed convection conditions.

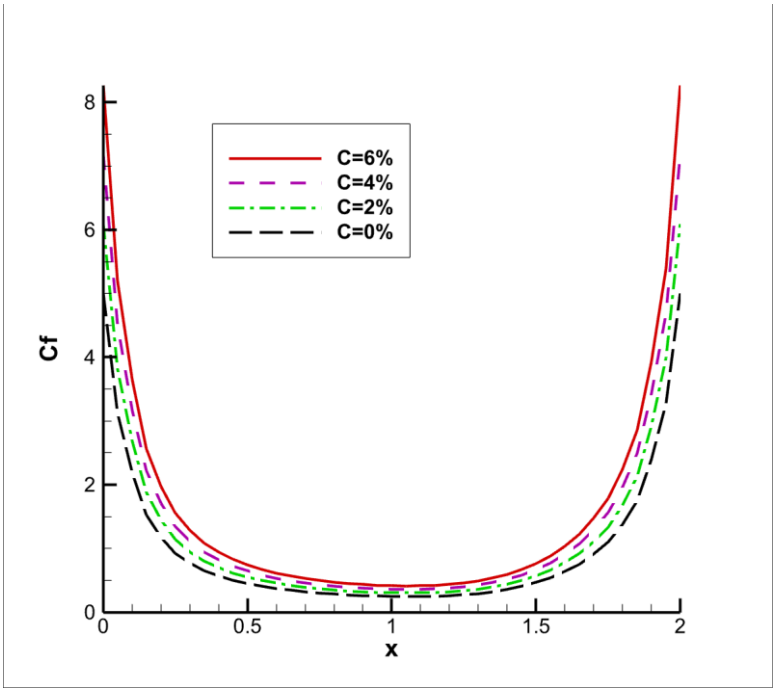


Figure 8. Local friction coefficient distribution along the bottom wall of the cavity for different ZnO nanoparticle volume fractions (ϕ=0%,2%,4%,6%).

Table 2 summarizes the average Nusselt number (Nu_{av}) and average friction coefficient (f_{av}) on the top and bottom walls of the cavity for nanoparticle volume fractions of φ = 0%, 2%, 4%, and 6%. These averaged quantities provide a quantitative measure of the overall thermal and hydrodynamic performance of the cavity under the combined effects of wall motion and buoyancy.

Regarding the thermal performance, the average Nusselt number on the top wall ($Nu_{av,top}$) increases monotonically with nanoparticle concentration, rising from 11.16 for pure water to 11.30, 11.59, and 11.87 for φ = 2%, 4%, and 6%, respectively. This monotonic enhancement, corresponding to an overall increase of about 6.4%, is attributed to the higher thermal conductivity of the ZnO–water nanofluid, which promotes more effective heat conduction through the thermal boundary layer and strengthens the convective heat transfer along the top wall. In contrast, the average Nusselt number on the bottom wall ($Nu_{av,bottom}$) exhibits a non-monotonic and generally decreasing trend: it drops sharply from 8.48 for pure water to 7.16 at φ = 2%, then increases slightly to 7.38 at φ = 4% and 7.40 at φ = 6%. This behavior indicates that, on the bottom wall, the adverse effects of increased viscosity and reduced thermal diffusivity outweigh the beneficial effect of enhanced thermal conductivity, particularly at low concentrations. The slight recovery at higher concentrations suggests a partial rebalancing between these competing mechanisms.

This opposing behavior highlights the asymmetric nature of heat transfer in the cavity, which arises from the different thermal and kinematic boundary conditions imposed on the top and bottom walls.

From a hydrodynamic perspective, the average friction coefficient (f_{av}) increases consistently with nanoparticle loading, rising from 1.00 for pure water to 1.22, 1.43, and 1.65 for φ = 2%, 4%, and 6%, respectively. This monotonic rise reflects the higher effective viscosity of the nanofluid, which intensifies the wall shear stress and increases the hydrodynamic penalty. It should be noted that the values of $f_{av,top}$ and $f_{av,bottom}$ appear identical in the table due to rounding to two decimal places; in the actual computations, slight differences exist in the higher decimal digits, reflecting the different flow structures and shear stress distributions on the two horizontal walls. Nevertheless, the overall magnitude and the trend of f_{av} are very similar for the top and bottom walls, indicating that the wall motion and the no-slip condition produce comparable levels of average shear stress despite their opposite directions.

Overall, the results in Table 2 demonstrate a clear trade-off between thermal enhancement and hydrodynamic penalty: while higher nanoparticle concentrations improve heat transfer on the top wall, they also increase the friction coefficient on both walls and reduce heat transfer on the bottom wall. These findings provide useful guidance for optimizing the nanoparticle concentration in mixed convection applications where both thermal performance and pumping power are of interest.

Table 2. Comparison of the average Nusselt number and average friction coefficient on the top and bottom walls for ϕ=0%,2%,4%, and 6% at *Re*=16, *Gr*=4, and *Pr*=6.161.

φ (%)	$Nu_{av,top}$	$Nu_{av,bottom}$	$f_{av,top}$	$f_{av,bottom}$
0 (pure water)	11.16	8.48	1.00	1.00
2	11.30	7.16	1.22	1.22
4	11.59	7.38	1.43	1.43
6	11.87	7.40	1.65	1.65

4. Conclusions

In this study, steady, two-dimensional, laminar mixed convection of a ZnO–water nanofluid in a rectangular cavity with an aspect ratio of 2 was numerically investigated. The upper and lower

horizontal walls moved in opposite directions and were maintained at different temperatures, while the vertical sidewalls were stationary and adiabatic. The governing equations were solved using a characteristic-based numerical method combined with artificial compressibility. The simulations were performed at Re = 16, Gr = 4, and Pr = 6.161, with the Eckert number set to zero. The effects of nanoparticle volume fractions of 0%, 2%, 4%, and 6% on local and average heat transfer and wall friction were examined.

The main contribution of this study is the comparative evaluation of the thermal and hydrodynamic responses of the two oppositely moving walls. Unlike an assessment based solely on the overall heat transfer rate, the present analysis separately examines the behavior of the hot and cold walls and demonstrates that nanoparticle addition can produce different thermal effects at these boundaries. The main findings are summarized as follows:

1. **Heat transfer along the upper wall:** The local Nusselt number decreases from the left corner toward the right corner. However, increasing the nanoparticle volume fraction systematically enhances the local heat transfer rate along this wall. The average Nusselt number increases from 11.16 for pure water to 11.87 at a nanoparticle concentration of 6%, representing an enhancement of approximately 6.4%.

2. **Heat transfer along the lower wall:** In contrast to the upper wall, the local Nusselt number generally decreases with increasing nanoparticle concentration. The average Nusselt number drops from 8.48 for pure water to 7.16 at 2% concentration, followed by a slight increase to 7.38 and 7.40 at 4% and 6%, respectively. This behavior indicates that the beneficial effect of enhanced thermal conductivity is counteracted by increased viscosity and reduced thermal diffusivity.

3. **Wall friction characteristics:** The local friction coefficient exhibits a U-shaped distribution along both horizontal walls, with maximum values near the corners and a minimum around the central region. Increasing the nanoparticle concentration consistently increases the friction coefficient because of the higher effective viscosity of the nanofluid. The average friction coefficient rises from 1.00 for pure water to 1.65 at 6% concentration.

4. **Thermal–hydrodynamic trade-off:** The results demonstrate that increasing the nanoparticle concentration does not provide a uniform improvement in the thermal performance of both walls. Although heat transfer is enhanced along the upper wall, it is generally reduced along the lower wall, while wall friction increases on both surfaces. This finding highlights the importance of considering the thermal and hydrodynamic responses of individual boundaries rather than relying exclusively on an overall heat transfer indicator.

Overall, the present investigation provides a configuration-specific understanding of how ZnO nanoparticle concentration influences mixed convection in a rectangular cavity with oppositely moving and differentially heated walls. The comparison of the two wall responses constitutes the main contribution of this work and provides useful information for evaluating the thermal benefits against the associated hydrodynamic penalties. The study is limited to a single set of Reynolds and Grashof numbers, a fixed cavity aspect ratio, and a single-phase nanofluid model. Future investigations may consider a wider range of flow parameters, different cavity geometries, three-dimensional configurations, and alternative nanoparticle materials to further explore the mechanisms identified in this study.

.

References

1. Eastman, J. A., Phillpot, S. R., Choi, S. U. S., & Keblinski, P. (2004). Thermal transport in nanofluids. Annual Review of Materials Research, 34, 219–246. https://doi.org/10.1146/annurev.matsci.34.052803.090621

2. Wang, X. Q., & Mujumdar, A. S. (2007). Heat transfer characteristics of nanofluids: A review. International Journal of Thermal Sciences, 46(1), 1–19. https://doi.org/10.1016/j.ijthermalsci.2006.06.010

3. Buongiorno, J. (2006). Convective transport in nanofluids. Journal of Heat Transfer, 128(3), 240–250. https://doi.org/10.1115/1.2150834

4. Choi, S. U. S. (2009). Nanofluids: From vision to reality through research. Journal of Heat Transfer, 131(3), 033106. https://doi.org/10.1115/1.3056479

5. Izadi, S., Armaghani, T., Ghasemiasl, R., Chamkha, A. J., & Molana, M. (2019). A comprehensive review on mixed convection of nanofluids in various shapes of enclosures. Powder Technology, 343, 880–907. https://doi.org/10.1016/j.powtec.2018.11.006

6. Muthtamilselvan, M., Kandaswamy, P., & Lee, J. (2010). Heat transfer enhancement of copper-water nanofluids in a lid-driven enclosure. Communications in Nonlinear Science and Numerical Simulation, 15(6), 1501–1510. https://doi.org/10.1016/j.cnsns.2009.06.015

7. Jmai, R., Ben-Beya, B., & Lili, T. (2016). Numerical analysis of mixed convection at various walls speed ratios in two-sided lid-driven cavity partially heated and filled with nanofluid. Journal of Molecular Liquids, 221, 691–713. https://doi.org/10.1016/j.molliq.2016.05.076

8. Boulahia, Z., Wakif, A., & Sehaqui, R. (2016). Numerical study of mixed convection of the nanofluids in two-sided lid-driven square cavity with a pair of triangular heating cylinders. Journal of Engineering, 2016, Article 8962091. https://doi.org/10.1155/2016/8962091

9. Rahmati, A. R., Roknabadi, A. R., & Abbaszadeh, M. (2016). Numerical simulation of mixed convection heat transfer of nanofluid in a double lid-driven cavity using lattice Boltzmann method. Alexandria Engineering Journal, 55(4), 3101–3114. https://doi.org/10.1016/j.aej.2016.08.017

10. Nazari, S., & Akbari, E. (2019). Numerical investigation of non-Newtonian nanofluid mixed convection in a two-opposite direction lid-driven cavity with variable properties. Heat Transfer—Asian Research, 48, 601–623. https://doi.org/10.1002/htj.21397

11. Keklikcioğlu Çakmak, N., Durmazuçar, H. H., & Yapıcı, K. (2020). A numerical study of mixed convection heat transfer in a lid-driven cavity using Al_2O_3-water nanofluid. International Journal of Chemistry and Technology, 4(1), 22–37. https://doi.org/10.32571/ijct.697728

12. Valizadeh Ardalan, M., Alizadeh, R., Fattahi, A., Adelian Rasi, N., Doranehgard, M. H., & Karimi, N. (2021). Analysis of unsteady mixed convection of Cu–water nanofluid in an oscillatory, lid-driven enclosure using lattice Boltzmann method. Journal of Thermal Analysis and Calorimetry, 145(4), 2045–2061. https://doi.org/10.1007/s10973-020-09789-3

13. Aljabair, S., Ekaid, A. L., Ibrahim, S. H., & Alesbe, I. (2021). Mixed convection in sinusoidal lid driven cavity with non-uniform temperature distribution on the wall utilizing nanofluid. Heliyon, 7(5), e06907. https://doi.org/10.1016/j.heliyon.2021.e06907

14. Alsabery, A. I., Tayebi, T., Kadhim, H. T., Ghalambaz, M., Hashim, I., & Chamkha, A. J. (2021). Impact of two-phase hybrid nanofluid approach on mixed convection inside wavy lid-driven cavity having localized solid block. Journal of Advanced Research, 30, 63–74. https://doi.org/10.1016/j.jare.2020.09.008

15. Nawafleh, A. S., Taamneh, Y., & Bataineh, K. (2023). Combined convection heat transfer in a lid-driven cavity filled with nanofluids. Heat Transfer, 52(1), 526–547. https://doi.org/10.1002/htj.22705

16. Souayeh, B. (2025). Numerical analysis of magnetohydrodynamics mixed convection and entropy generation in a double lid-driven cavity using ternary hybrid nanofluids. Advanced Theory and Simulations, 8(5), 2401357. https://doi.org/10.1002/adts.202401357

17. Mliki, B., Ferhi, M., & Abbassi, M. A. (2025). Numerical study of MHD mixed convection of nanofluid flow in a double lid convergent cavity. Acta Mechanica et Automatica, 19(2), 232–242. https://doi.org/10.2478/ama-2025-0029

18. Loukopoulos, V. C., Bourantas, G. C., Georgopoulos, V. P., & Burganos, V. N. (2026). Mixed convective two phase flow of an electrically conducting micropolar nanofluid in a double lid-driven square cavity. International Journal of Thermofluids, 31, 101508. https://doi.org/10.1016/j.ijft.2025.101508

19. Cao, Y., Almasi, H., Soto, C., Akbari, O. A., Ahmadi, G., Esmaeili, S., & Khairy, Y. (2025). Mixed convection of nanofluid flow in a circular lid-driven cavity affected by attack angle changes: A numerical simulation. Case Studies in Thermal Engineering, 75, 107111. https://doi.org/10.1016/j.csite.2025.107111

20. Adibi, T., Razavi, S. E., Adibi, O., Vajdi, M., & Sadegh Moghanlou, F. (2021). The response of nano-ceramic doped fluids in heat convection models: A characteristics-based numerical approach. Scientia Iranica, 28(5), 2671–2683. https://doi.org/10.24200/sci.2021.56574.4794